Original Article

Institution of MECHANICAL ENGINEERS

Journal of MECHANICAL ENGINEERING SCIENCE

Proc IMechE Part C:
J Mechanical Engineering Science
2019, Vol. 233(1) 302–312

DOI: 10.1177/0954406218756938
journals.sagepub.com/home/pic

SAGE

Prediction of residual clamping force for Coulomb type and Johnsen–Rahbek type of bipolar electrostatic chucks

Kesheng Wang, Yijia Lu, Jia Cheng and Linhong Ji

Abstract

As a key component in semiconductor manufacturing equipment, electrostatic chuck is conventionally divided into Coulomb type and J–R type depending on the generating mechanism of clamping force. After supply voltage is cut off, residual clamping force usually remains and becomes a serious issue for production efficiency and process reliability. Hence, it is significant to propose a general prediction model and reveal changing laws of residual force with time for both types. This paper establishes an equivalent circuit model for a bipolar electrostatic chuck containing distributed embosses on dielectric layer surface, and deduces a unified form of mathematical expression describing decaying force, which can cover the two types. The obtained equations can also predict steady force in working state. Furthermore, an experimental method for measuring clamping force and de-clamping time is presented. The results indicate relative deviations tend to decrease as voltages rise. It is found that prediction precision for J–R type is lower than that for Coulomb type. Main reasons are explained and relevant mechanisms are discussed. Overall, the calculations coincide with the measurements within an acceptable error range. The comparisons suggest the theoretical model is effective for simulating the characteristics of residual clamping force for both types of electrostatic chucks.

Keywords

Semiconductor manufacturing, silicon wafer, electrostatic chuck, residual clamping force, Coulomb type, Johnsen–Rahbek type

Date received: 3 March 2017; accepted: 8 January 2018

Introduction

Electrostatic chucks are being widely used in semiconductor manufacturing equipment. In particular, an electrostatic chuck is an indispensable component for a dry etcher or chemical-vapor deposition (CVD) apparatus. It is clear that the clamping force is one of the most important factors influencing the effectiveness of an electrostatic chuck,[1–5] which can directly or indirectly influence other key parameters including wafer temperature, wafer flatness, and so on.

The clamping force is conventionally classified into two categories depending on its mechanism. One is Coulomb force,[6–8] which is dominant when the resistivity of the dielectric layer is relatively high. The force is due to the polarized charge that is induced by the electric field between the electrode and the wafer. The other is Johnsen–Rahbek (J–R) force,[9–12] which is dominant when the resistivity of the dielectric layer is relatively low. The force is induced from the free charge stored in the narrow gap between the wafer backside and the dielectric layer surface, due to the surface roughness. Generally speaking, this type of electrostatic chuck can generate higher clamping force.

After the wafer processing is finished, the voltage applied on the electrostatic chuck must be cut off immediately. As mentioned in the previous literature,[13–23] the residual clamping force resulted from the residual charges usually remains. It has become a serious issue for production efficiency and process reliability. Long de-clamping time can either reduce the throughput or cause the wafer breakage during the wafer unloading cycle dependent on the wafer lifting mechanism. Accordingly, it is essential to reveal the changing laws of the residual clamping

State Key Laboratory of Tribology, Department of Mechanical Engineering, Tsinghua University, Beijing, China

Corresponding author:
Jia Cheng, State Key Laboratory of Tribology, Department of Mechanical Engineering, Tsinghua University, Beijing 100084, China.
Email: chengjia@tsinghua.edu.cn

force with time and construct the theoretical prediction model.

There are a large number of patents dealing with the elimination of the residual clamping force. Nevertheless, few scientific papers concerning theoretical modeling for the residual clamping force have been published. On the other hand, the previous works emphasized the difference between Coulomb type and J–R type, and regarded them as two quite distinct systems.[14,19–21,23] In fact, the clamping forces for all types of electrostatic chucks combine Coulomb force and J–R force to some extent,[15] and they are bound to have some characteristics in common. Therefore, it is possible and significant to seek an approach to unify the mathematical expression of the electrostatic force for both types of electrostatic chucks.

In this paper, we focused on establishing a uniform mathematical model predicting the residual clamping force or the de-clamping time after the power supply voltage was cut off, which can cover Coulomb type and J–R type. A novel method for in situ measuring the residual clamping force and the corresponding time was proposed to confirm the validity of the theoretical model.

Figure 1. Photo of an electrostatic chuck.

Theoretical modeling

Figure 1 shows a bipolar electrostatic chuck as the object of this study. Two spiral electrodes are illustrated in Figure 2. The positive electrode and the negative electrode can be interdigitated each other. Generally speaking, they almost have the same area. The fundamental structure of the electrostatic chuck is schematically shown in Figure 3. A number of embosses are uniformly distributed on the surface of the dielectric layer. Although there are opposite charges on the positive and negative electrodes, respectively, they both produce the electrostatic attractive force on the wafer. However, the area without electrode involved doesn't contribute to the electrostatic force. Despite the different pattern of electrode, the fundamental structure can be divided into lots of unit structure as shown in Figure 4, which comprises two kind of typical features, emboss and gap. The dimension of unit structure is the order of submillimeter, which is tiny enough compared with the width of the electrode. As a result, we proposed a unit model, which could be integrated statistically over the electrode of the whole electrostatic chuck, no matter what pattern. The space between the electrode and the wafer can be divided into four parts including the bulk, the gap, the pillar, and the contact interface stemmed from the asperities. In Figure 4, d denotes the thickness of the bulk, h denotes the height of the emboss, and δ denotes the average thickness of the contact interface, relevant to the surface roughness. Apparently, the thickness of the pillar is $d+h$, and the thickness of the gap is $h+\delta$.

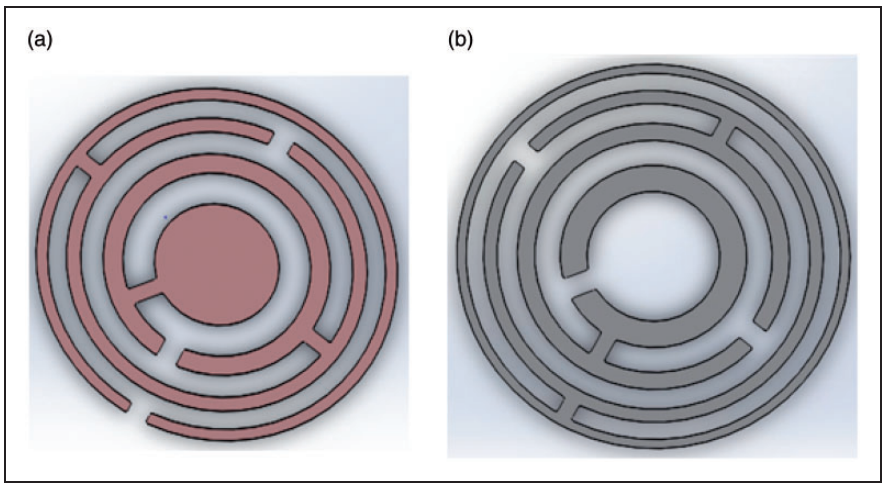

Figure 2. Configuration of spirally interdigitated electrodes: (a) positive electrode; (b) negative electrode.

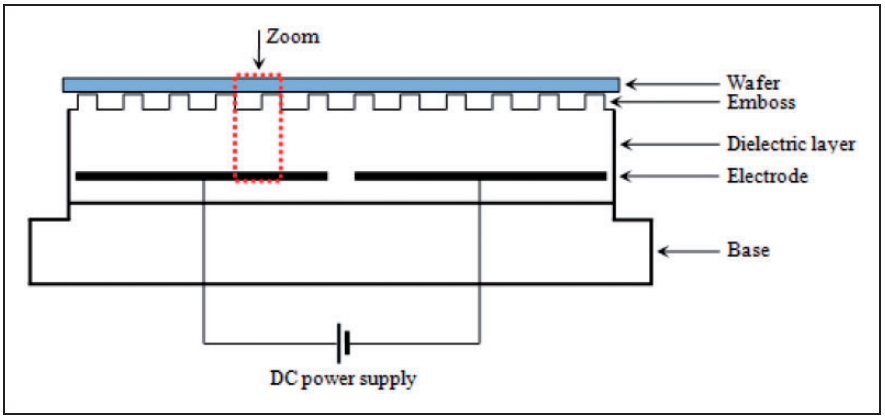

Figure 3. Fundamental structure of a bipolar electrostatic chuck.

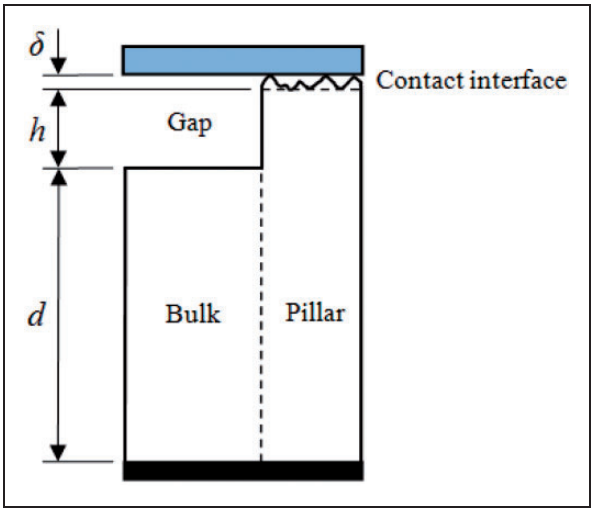

Figure 4. Enlarged view of unit structure.

According to the principle of equal potential, we established a set of equivalent circuit for the Coulomb-type bipolar electrostatic chuck in working state, as shown in Figure 5. Note that the resistance of the wafer is negligible because the resistivity of silicon wafer, ranging from 2 to 50 Ω·cm, is small enough compared with that of the dielectric layer (typically, 10^7–10^{13} Ω·cm). The wafer and the electrode are considered as the two equipotential nodes, respectively. Hence, the equivalent circuit can be regarded as bilateral symmetry. The electric parameters of the circuit model are given in Figure 5.

In this case, the air gap above the bulk zone results in the open circuit. Therefore, the resistance of bulk is absent in this branch of the equivalent circuit. The capacitance of the bulk C_{bulk} can be determined by

$$C_{\text{bulk}} = \varepsilon_0 \varepsilon_{\text{d}} \frac{\varphi A(1-\eta)}{d} \tag{1}$$

where ε_0 is the dielectric constant of the vacuum, ε_{d} is the relative dielectric constant of the dielectric layer, φ is the area ratio of the positive or negative electrode to the dielectric layer, A is the total area of the dielectric layer, and η is the area ratio of all embosses to the dielectric layer.

The capacitance of the gap C_{gap} can be determined by

$$C_{\text{gap}} = \varepsilon_0 \varepsilon_{\text{g}} \frac{\varphi A(1-\eta)}{h+\delta} \tag{2}$$

where ε_{g} is the relative dielectric constant of the gas inside the gap or the contact interface.

The capacitance of the pillar C_{pillar} can be determined by

$$C_{\text{pillar}} = \varepsilon_0 \varepsilon_{\text{d}} \frac{\varphi A \eta}{d+h} \tag{3}$$

The capacitance of the contact interface C_{contact} can be approximately determined by

$$C_{\text{contact}} = \varepsilon_0 \varepsilon_{\text{g}} \frac{\varphi A \eta}{\delta} \tag{4}$$

The capacitance is determined by the area, gap and relative permittivity, and hardly changes with the surface topography of the contact region.

The resistance of the pillar R_{pillar} can be determined by

$$R_{\text{pillar}} = \rho_{\text{d}} \frac{d+h}{\varphi A \eta} \tag{5}$$

where ρ_{d} is the resistivity of the dielectric layer.

It is very difficult to accurately calculate the resistance of the contact interface R_{contact} due to the high complexity of the contact status. In this case, the situation at the contact interface has significant influence on the resistance, because there are more asperities between the wafer and the dielectric. The charges can transfer more easily, resulting in the lower resistance. The value can be estimated by the following empirical formula[24]

$$R_{\text{contact}} = \frac{\rho_{\text{d}} + \rho_{\text{w}}}{2} \sqrt{\frac{\min(H_{\text{d}}, H_{\text{w}})}{F_{\text{contact}}}} \tag{6}$$

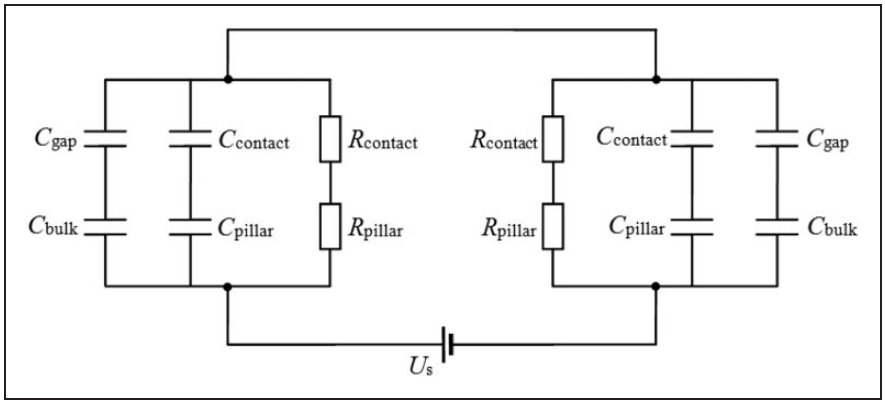

Figure 5. Equivalent circuit model of Coulomb-type bipolar electrostatic chuck in working state.

where ρ_w is the resistivity of the wafer, H_d is the hardness of the dielectric layer, H_w is the hardness of the wafer, and $F_{contact}$ is the contact force. Obviously, the contact resistance $R_{contact}$ is not a constant and it will change with the contact force. As a result, the voltage of the $R_{contact}$ is not equal to that of $C_{contact}$.

When C_{bulk} and C_{gap} are connected in series, the equivalent capacitance C_1 is expressed as

$$C_1 = \frac{1}{\frac{1}{C_{bulk}} + \frac{1}{C_{gap}}} = \varepsilon_0 \varepsilon_d \varepsilon_g \frac{\varphi A(1-\eta)}{d\varepsilon_g + (h+\delta)\varepsilon_d} \tag{7}$$

When C_{pillar} and $C_{contact}$ are connected in series, the equivalent capacitance C_2 is expressed as

$$C_2 = \frac{1}{\frac{1}{C_{pillar}} + \frac{1}{C_{contact}}} = \varepsilon_0 \varepsilon_d \varepsilon_g \frac{\varphi A \eta}{(d+h)\varepsilon_g + \delta\varepsilon_d} \tag{8}$$

Then, the shunt capacitance C of C_1 and C_2 is expressed as

$$\begin{aligned} C &= C_1 + C_2 \\ &= \varepsilon_0 \varepsilon_d \varepsilon_g \varphi A \left[\frac{1-\eta}{d\varepsilon_g + (h+\delta)\varepsilon_d} + \frac{\eta}{(d+h)\varepsilon_g + \delta\varepsilon_d} \right] \end{aligned} \tag{9}$$

When R_{pillar} and $R_{contact}$ are connected in series, the equivalent resistance R is expressed as

$$R = R_{pillar} + R_{contact} \tag{10}$$

Note that $\rho_d \gg \rho_w$, and $H_d > H_w$, we can obtain the following equation from equations (5) and (6).

$$\frac{R_{contact}}{R_{pillar}} = \frac{\varphi A \eta}{2(d+h)} \sqrt{\frac{H_w}{F_{contact}}} \tag{11}$$

If we assume that $\varphi = 0.43$, $A = 679\,\text{cm}^2$, $\eta = 0.37$, $d = 300\,\mu\text{m}$, $h = 10\,\mu\text{m}$, $H_w = 10.2\,\text{GPa}$, and $F_{contact} = 0.1 \sim 100\,\text{N}$, the calculation result shows that $R_{contact} \gg R_{pillar}$, which means R_{pillar} can be neglected. Thus equation (10) turns into

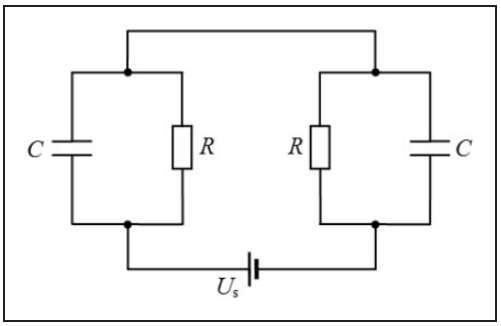

Figure 6. Simplified equivalent circuit model in working state.

$$R = R_{contact} = \frac{\rho_d}{2} \sqrt{\frac{H_w}{F_{contact}}} \tag{12}$$

The simplified equivalent circuit in working state is shown in Figure 6. The applied voltage U corresponding to each equivalent capacitance C is determined by

$$U = \frac{U_s}{2} \tag{13}$$

where U_s is the DC supply voltage.

After the supply voltage is cut off, the equivalent circuit model is illustrated in Figure 7. The left and right capacitors are discharged in the respective local circuit, without interfering with each other. Next, we only select the left part to analyze the discharge process due to the topological symmetry.

According to the fundamental theory of electric circuits, we can easily derive the following equation

$$u = \frac{U_s}{2} e^{-\frac{1}{RC}t} \tag{14}$$

where u is the transient voltage between the wafer and either of the electrodes, and t is time.

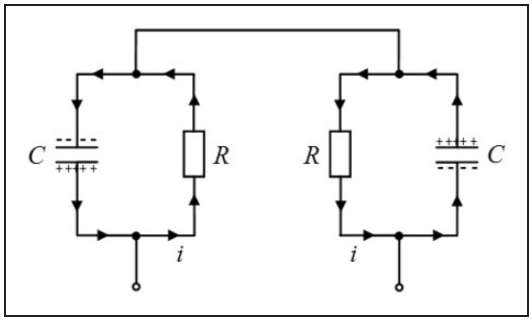

Figure 7. Discharge circuit after cutting off supply voltage.

Equation (14) describes the exponentially decaying voltage with time, applied between the electrode and the wafer, after the DC supply voltage is cut off. Then, based on the calculation principle of Coulomb force,[15,16,25] we can deduce the total residual clamping force F_{re} generated by the electrostatic chuck. According to the unit structure shown in Figure 4, the residual clamping force derives from two parts of electrostatic attractive force. One is generated by the electrode under the pillar, called $F_{contact}$, and the other is generated by the electrode under the bulk, called $F_{noncontact}$.

For the right part of the unit structure shown in Figure 4, it can be regarded as two capacitors connected serially. Therefore, the residual clamping force $F_{contact}$ can be expressed as[15]

$$F_{contact} = \varphi A \eta \varepsilon_0 \left[\frac{\varepsilon_d \varepsilon_g}{(d+h)\varepsilon_g + \delta\varepsilon_d} u \right]^2 \tag{15}$$

Similarly, for the left part of the unit structure shown in Figure 4, it can also be regarded as two capacitors connected serially. Therefore, the residual clamping force $F_{noncontact}$ can be expressed as[15]

$$F_{noncontact} = \varphi A (1-\eta) \varepsilon_0 \left[\frac{\varepsilon_d \varepsilon_g}{d\varepsilon_g + (h+\delta)\varepsilon_d} u \right]^2 \tag{16}$$

Thus the total residual clamping force F_{re} is

$$\begin{aligned} F_{re} &= F_{contact} + F_{noncontact} \\ &= \varphi A \eta \varepsilon_0 \left[\frac{\varepsilon_d \varepsilon_g}{(d+h)\varepsilon_g + \delta\varepsilon_d} u \right]^2 \\ &\quad + \varphi A (1-\eta) \varepsilon_0 \left[\frac{\varepsilon_d \varepsilon_g}{d\varepsilon_g + (h+\delta)\varepsilon_d} u \right]^2 \\ &= \varepsilon_0 \varepsilon_d^2 \varepsilon_g^2 \varphi A \\ &\quad \times \left\{ \frac{\eta}{\left[(d+h)\varepsilon_g + \delta\varepsilon_d\right]^2} + \frac{1-\eta}{\left[d\varepsilon_g + (h+\delta)\varepsilon_d\right]^2} \right\} u^2 \end{aligned} \tag{17}$$

where the first term corresponds to the noncontact parts (without emboss), and the second term corresponds to the contact parts (with emboss).

According to the ratio of the two terms, the contact force between the emboss and the wafer can be calculated by the following equation

$$F_{contact} = \frac{1}{2} F_{re} \frac{\eta\left[d\varepsilon_g + (h+\delta)\varepsilon_d\right]^2}{\left\{ \begin{array}{c} (1-\eta)\left[(d+h)\varepsilon_g + \delta\varepsilon_d\right]^2 \\ + \eta\left[d\varepsilon_g + (h+\delta)\varepsilon_d\right]^2 \end{array} \right\}} \tag{18}$$

Note that only the contact force corresponding to the positive electrode is involved in equation (18), because both of the electrodes generate the same electrostatic force.

Plugging equation (18) into equation (12), we can obtain

$$R = \frac{\rho_d}{2} \sqrt{\frac{2H_w \left\{ \begin{array}{c} (1-\eta)\left[(d+h)\varepsilon_g + \delta\varepsilon_d\right]^2 \\ + \eta\left[d\varepsilon_g + (h+\delta)\varepsilon_d\right]^2 \end{array} \right\}}{\eta\left[d\varepsilon_g + (h+\delta)\varepsilon_d\right]^2 F_{re}}} \tag{19}$$

Plugging equation (14) into equation (17), we can obtain

$$\begin{aligned} F_{re} = \varepsilon_0 \varepsilon_d^2 \varepsilon_g^2 \varphi A \Bigg\{ &\frac{1-\eta}{\left[d\varepsilon_g + (h+\delta)\varepsilon_d\right]^2} \\ &+ \frac{\eta}{\left[(d+h)\varepsilon_g + \delta\varepsilon_d\right]^2} \Bigg\} \frac{U_s^2}{4} e^{-\frac{2}{RC}t} \end{aligned} \tag{20}$$

Based on equations (9) and (19), the following expression is given

$$\begin{aligned} \frac{2}{RC} = &\frac{4\left[d\varepsilon_g + (h+\delta)\varepsilon_d\right]}{\rho_d \varepsilon_0 \varepsilon_d \varepsilon_g \varphi A \left[\begin{array}{c} \dfrac{1-\eta}{d\varepsilon_g + (h+\delta)\varepsilon_d} \\ + \dfrac{\eta}{(d+h)\varepsilon_g + \delta\varepsilon_d} \end{array} \right]} \\ &\cdot \sqrt{\frac{\eta F_{re}}{2H_w \left\{ \begin{array}{c} (1-\eta)\left[(d+h)\varepsilon_g + \delta\varepsilon_d\right]^2 \\ + \eta\left[d\varepsilon_g + (h+\delta)\varepsilon_d\right]^2 \end{array} \right\}}} \end{aligned} \tag{21}$$

According to equations (20) and (21), we deduce such an implicit function as

$$F_{re} = F_0 e^{-\beta t \sqrt{F_{re}}} \tag{22}$$

where the residual clamping force F_{re} is a function of time t, and F_0 and β are the introduced coefficients expressed by

$$F_0 = \frac{1}{4} \varepsilon_0 \varepsilon_d^2 \varepsilon_g^2 \varphi A$$

$$\times \left\{ \frac{1-\eta}{\left[\mathrm{d}\varepsilon_{\mathrm{g}} + (h+\delta)\varepsilon_{\mathrm{d}}\right]^2} + \frac{\eta}{\left[(d+h)\varepsilon_{\mathrm{g}} + \delta\varepsilon_{\mathrm{d}}\right]^2} \right\} U_{\mathrm{s}}^2 \tag{23}$$

$$\beta = \frac{4\left[d\varepsilon_{\mathrm{g}} + (h+\delta)\varepsilon_{\mathrm{d}}\right]}{\rho_{\mathrm{d}}\varepsilon_0\varepsilon_{\mathrm{d}}\varepsilon_{\mathrm{g}}\varphi A\left[\begin{array}{c} \dfrac{1-\eta}{d\varepsilon_{\mathrm{g}} + (h+\delta)\varepsilon_{\mathrm{d}}} \\ + \dfrac{\eta}{(d+h)\varepsilon_{\mathrm{g}} + \delta\varepsilon_{\mathrm{d}}} \end{array}\right]} \cdot \sqrt{\frac{\eta F_{\mathrm{re}}}{2H_{\mathrm{w}}\left\{\begin{array}{c} (1-\eta)\left[(d+h)\varepsilon_{\mathrm{g}} + \delta\varepsilon_{\mathrm{d}}\right]^2 \\ + \eta\left[d\varepsilon_{\mathrm{g}} + (h+\delta)\varepsilon_{\mathrm{d}}\right]^2 \end{array}\right\}}} \tag{24}$$

After cutting off the supply voltage, the mathematical model predicting the decaying electrostatic force with time is established by equations (22) to (24).

For Coulomb-type chucks, the above theoretical equations can be used directly. For J–R-type chucks, some crucial revisions will be indispensable. On the one hand, due to the lower dielectric resistivity, the resistance of the dielectric layer is sufficiently small compared with that of the gap or the contact interface, so that it can be approximated to zero. On the other hand, the capacitance of the dielectric layer is sufficiently large compared with that of the gap or the contact interface, so that it can be approximated to infinity. Thus, it is equivalent to removing the pillar resistance R_{pillar}, the bulk capacitance C_{bulk} and the pillar capacitance C_{pillar} shown in Figure 5, and they are replaced by conductive wires. This means that both the bulk thickness d and the pillar thickness $d+h$, marked in Figure 4, drop to zero. In equations (23) and (24), if $d=0$ and $d+h=0$ (note that $h \neq 0$), we can obtain the simplified expressions as

$$F_0 = \frac{1}{4}\varepsilon_0\varepsilon_{\mathrm{g}}^2\varphi A\left[\frac{1-\eta}{(h+\delta)^2} + \frac{\eta}{\delta^2}\right] U_{\mathrm{s}}^2 \tag{25}$$

$$\beta = \frac{4(h+\delta)}{\rho_{\mathrm{d}}\varepsilon_0\varepsilon_{\mathrm{g}}\varphi A\left(\frac{1-\eta}{h+\delta} + \frac{\eta}{\delta}\right)} \sqrt{\frac{\eta}{2H_{\mathrm{w}}\left[(1-\eta)\delta^2 + \eta(h+\delta)^2\right]}} \tag{26}$$

Equations (22), (25), and (26) are the mathematical model predicting the decaying electrostatic force with time after cutting off the supply voltage, which can be applicable to the J–R type. It should be pointed out that although the generating mechanisms of Coulomb force and J–R force are somewhat different, the calculation models for the two types of clamping force have a unified form in nature. The corresponding J–R force model can be obtained by adjusting some specific parameters in the Coulomb force model. Consequently, from the view of mathematical expression, the equation of electrostatic force for the J–R type can be regarded as a special case of that for the Coulomb type. In addition, the physical significance has also been elaborated above.

At the same time, we find that the introduced coefficient F_0 in equation (22) is the initial clamping force at $t=0$, which suggests that the steady clamping force of electrostatic chuck in working state can also be calculated by equation (23) or equation (25). Therefore, the established mathematical model can predict the steady-state clamping force and the residual clamping force simultaneously, with a wider range of applications.

Experimental method

Measurement principle of clamping force in electrostatic chuck

Figure 8 shows the main principle of the experimental apparatus, which has been improved on the basis of our previous design.[26] Multiple micro-force probe components are adopted and each component consists of a precision linear feed mechanism, a micro-force sensor and a ruby probe. One of the probes is set to point at the wafer center and the others are uniformly distributed along the wafer circumference, so that more comprehensive experimental data can be acquired. The role of the linear feed mechanism is driving the probe to lift up and down. The tiny touch force between the probe and the wafer is monitored by the micro-force sensor. When it reaches a threshold value, the movement of the linear feed mechanism will be paused immediately to ensure that the touch force is far less than the clamping force. Thus the touch force can be considered to be approximately zero at this time.

Meanwhile, we introduce the pressurized gas flowing in the narrow space of the gap between the wafer and the dielectric layer. The support force between the wafer and the electrostatic chuck will gradually decrease with the increasing gas pressure. At the moment of de-clamping, the support force provided by the electrostatic chuck vanishes completely and the probe begins to provide the support force for the wafer, which will cause an abrupt rise of the touch force between the probe and the wafer. This means that the local de-clamping is occurring and the relevant criteria have been found. Hence, the touch force is selected as a key indicator to characterize de-clamping, and the moment of de-clamping can be exactly judged.

When the reading of any one of these micro-force sensors reaches a certain percentage of its full scale, we deem that the local de-clamping around the corresponding probe has occurred. The entire de-clamping will finish until the reading of each sensor respectively reaches the same percentage of its full

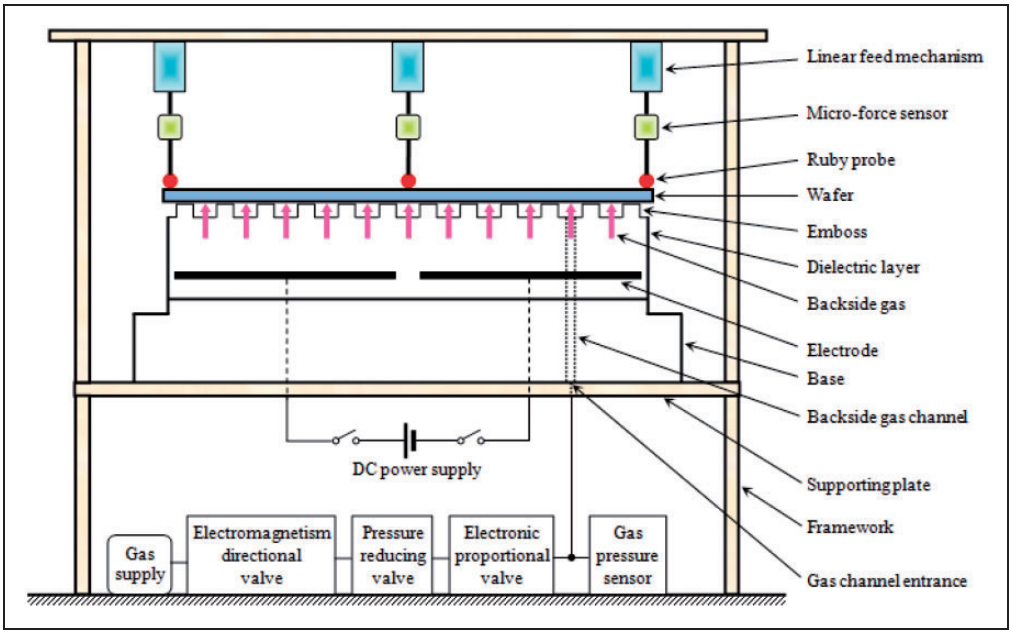

Figure 8. Schematic diagram of the experimental apparatus.

scale. Accordingly, we focus on the reading of the last sensor, and record the moment of entire de-clamping and the corresponding gas pressure. Because one of the measured parameters in the experiment is the gas pressure, it must be converted into the gas resultant force acting on the wafer backside by an appropriate area. After the local de-clamping occurs, the contact interface illustrated in Figure 4 will also be filled with the pressurized gas, so the actual acting area of the pressurized gas should be approximately regarded as the total area A of the dielectric layer. In accordance with the equilibrium equation, the clamping force for the electrostatic chuck is equal to the gas resultant force acting on the wafer backside, with ignoring the wafer weight.

Measurement method of residual clamping force

Now that we have determined the backside gas pressure p_0 at the moment of entire de-clamping, we can measure the residual clamping force after the DC supply voltage is cut off. Under normal working conditions of the electrostatic chuck, the backside gas pressure p_1 ($p_1 < p_0$) can be kept constant by feedback control of the flow rate. After cutting off the supply voltage, the residual clamping force will gradually decrease with time. When it drops to the gas resultant force of p_1, the de-clamping occurs, detected by the micro-force probe components, and the corresponding time t_1 can be recorded automatically. Obviously, the residual clamping force F_{re1} at the de-clamping time t_1 is $p_1 A$. In theory, we can set different backside gas pressure $p_1, p_2, \ldots, p_n$ lower than p_0, and a series of de-clamping time $t_1, \ldots t_2, \ldots, t_n$ will be measured. In this way, the correlation between the backside gas pressure, i.e. the residual clamping force and time can be given.

Table 1. Main parameters of Coulomb-type electrostatic chuck used in the experiments.

Parameter	ε_0 (F/cm)	ρ_d ($\Omega \cdot$ cm)	H_d (GPa)	H_w (GPa)	A (cm^2)	
Value	8.85×10^{-14}	2×10^{13}	18.5	10.2	679	
Parameter	d (μm)	h (μm)	δ (μm)	η	φ	ε_d	ε_g
Value	300	10	1.6	0.37	0.43	10	1

Comparison of theoretical calculations with experimental results

The experiments were performed on a self-designed measurement platform in atmospheric environment. We prepared a Coulomb-type chuck made of alumina and a J–R-type chuck made of aluminum nitride, respectively. They have the same geometrical sizes and working conditions, mainly differing in the resistivity of the dielectric layer. The relevant parameters of the Coulomb-type chuck used in the experiments are listed in Table 1. The dielectric resistivity ρ_d of the J–R-type chuck is about 2×10^7 cm.

Steady-state clamping force as a function of supply voltage

At first, we measured the steady clamping force in working state by altering the power supply voltage.

The comparisons between the measurements and calculations for the two chucks are plotted in Figure 9.

According to equations (23) or (25), the steady-state clamping force is proportional to the square of the supply voltage. It is found from Figure 9 that the basic trend of the experimental results agrees well with that of the theoretical curves. We notice that the measured values are smaller than the predicted ones, and the systematic error could be caused by an inevitable leakage of the pressurized gas between the wafer and the electrostatic chuck.

Furthermore, the errors gradually decrease with the growing supply voltages. In Figure 9(a), the mean error varies from 22.9% at 1000 V to 7.9% at 2800 V. In Figure 9(b), the mean error varies from 30.7% at 50 V to 9.5% at 350 V. The reason might be explained by the improvement of the contact condition due to the stronger clamping force at higher supply voltage.

Also, the global errors are 12.9% and 16.2% in the case of Coulomb type and J–R type, which means that the prediction precision of the steady-state clamping force for J–R type is lower than that for Coulomb type. This is because the J–R force is more sensitive to a slight change of the contact interface thickness, compared with the Coulomb force.[14,20] If the coupling relationship between the electrostatic force and the contact interface thickness can be described quantitatively and added to the theoretical model, the prediction accuracy will be further improved. The issue is challenging and has become one of our next subjects, requiring an in-depth study. On the other hand, J–R

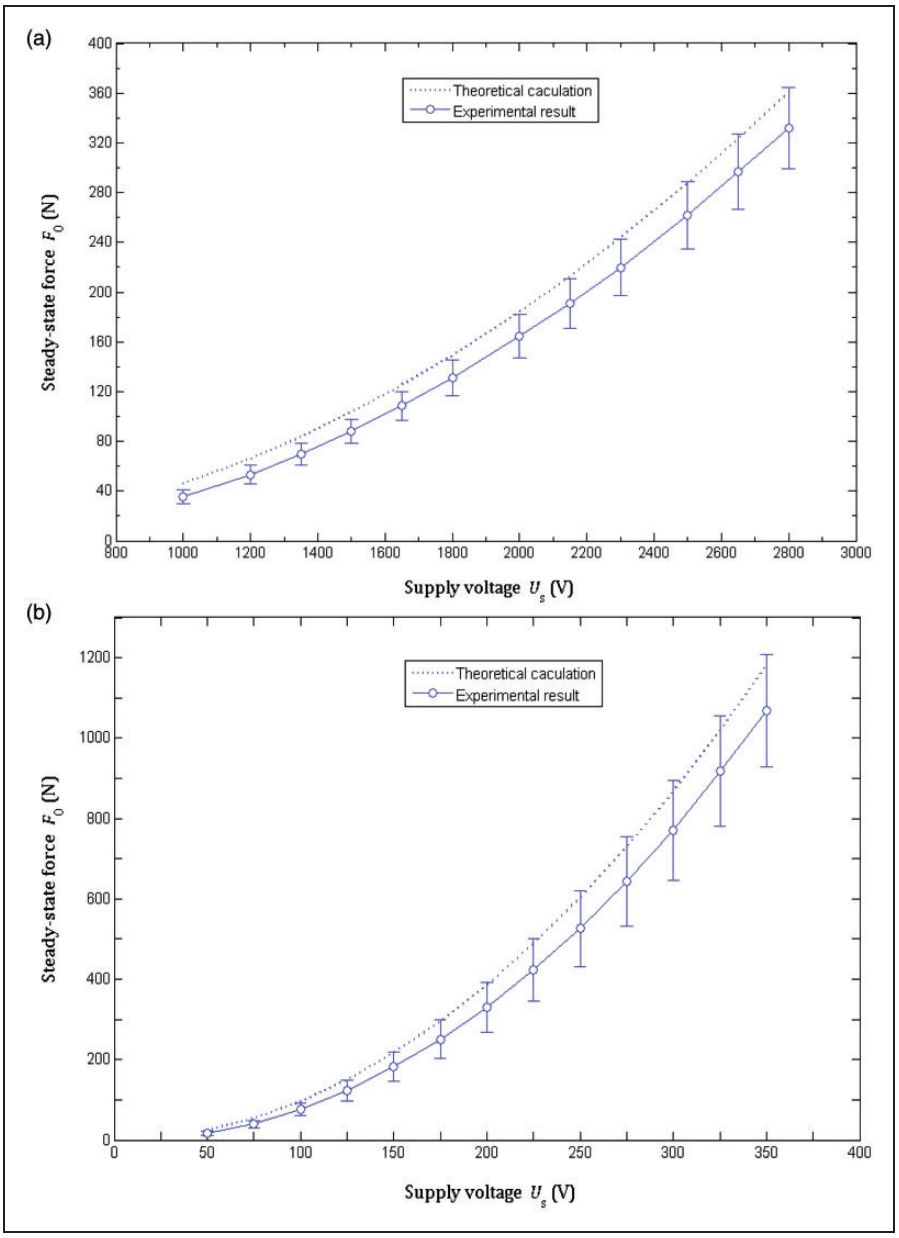

Figure 9. Steady-state clamping force versus power supply voltage: (a) Coulomb type; (b) J–R type.

effect can cause field emission of electrons under intense electric field,[27,28] contributing to reducing the prediction precision to some extent.

It should be pointed out that the supply voltage must be within a reasonable range. Its upper limit cannot exceed the breakdown voltage of the electrostatic chuck, and the maximum output gas pressure of electronic proportional valve should also be taken into account, or the de-clamping may not occur in the experiment. On the contrary, if the supply voltage is too low, the generated clamping force is so weak that the clamping effect will deteriorate, leading to unacceptable errors.

In conclusion, the comparisons suggest that the deduced mathematical model can be employed to predict the steady-state clamping force for both types of electrostatic chucks.

Residual clamping force as a function of time

After cutting off the power supply voltage, the residual clamping force will decline as the time elapses. The comparisons between the measurements and calculations for the two chucks are plotted in Figure 10, where the Matlab function, ezplot, is used to plot the curves of implicit function corresponding to equation (22).

Apparently, vastly different decaying time was observed in Figure 10(a) and (b). The former is much longer than the latter, which is attributed to the disparity of the dielectric resistivity. Thus, the migration and dissipation rate of the residual charges stored in the dielectric layer can greatly affect the decaying time of the clamping force. However, a common characteristic of the curves lies in that

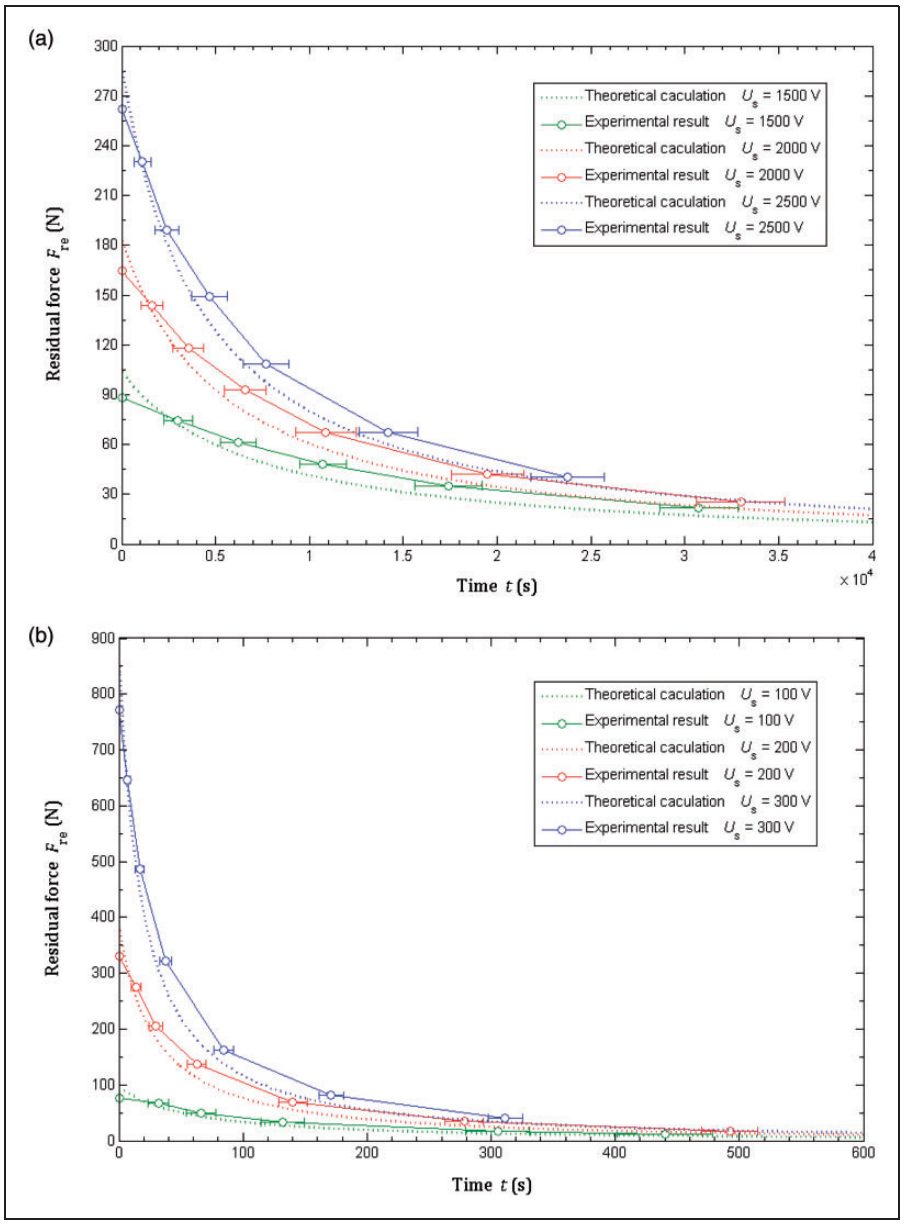

Figure 10. Residual clamping force versus time: (a) Coulomb type; (b) J–R type.

although the different clamping forces decrease at different rates after the supply voltages are cut off, the final residual clamping forces remain approximately constant and are almost equal, regardless of different initial voltages. This might result from the saturation of the charge migration and dissipation after a period of time.

From Figure 10, we can find that the tendency of the experimental results is consistent with that of the theoretical curves. During the decline of the curves, most the theoretical values drift to the left of the experimental data, which means that the calculated residual forces drop faster than the measured ones. Actually, before the de-clamping occurs, the real contact force between the emboss and the wafer is less than the predicted one due to the impact of the backside gas pressure, which in turn leads to the increase of the contact resistance. The result indicates that the experimentally measured de-clamping time is prolonged.

It is noted that the relative deviations between the measurements and calculations decrease with the rising supply voltages. In Figure 10(a), while $U_s = 1500$ V, 2000 V, and 2500 V, the average deviations are 28.4%, 20.9%, and 13.8%, respectively. In Figure 10(b), while $U_s = 100$ V, 200 V, and 300 V, the average deviations are 33.7%, 24.1%, and 18.5%, respectively. Such phenomenon can be attributed to a decline in gas leakage of the wafer backside owing to the compression by the stronger clamping force at higher supply voltage.

Moreover, the contrast demonstrates that the prediction precision of the residual clamping force for J–R type is usually lower than that for Coulomb type. The explanations are similar to the ones for the steady-state clamping force mentioned above.

To sum up, the comparisons indicate that the established theoretical model is reasonable and can reveal the changing laws of the residual clamping force with time for both types of electrostatic chucks.

Conclusions

This paper establishes an equivalent circuit model for a bipolar electrostatic chuck containing the distributed embosses on the dielectric layer surface, and derives an implicit function describing the decaying clamping force with time after cutting off the supply voltage. A unified form of the calculation models are presented and the equation for J–R type can be regarded as a special case of that for Coulomb type in terms of mathematical expression. Meanwhile, the theoretical formula can also predict steady clamping force in working state. We develop a novel experimental method to measure the clamping force and de-clamping time by adopting multiple micro-force probes, with the pressurized gas acting on the wafer backside. The comparisons between the measurements and calculations manifest that the steady-state clamping force is proportional to the square of the supply voltage, and the experimental results are smaller than the theoretical values, with the mean errors of 12.9% and 16.2% in the case of Coulomb type and J–R type, respectively. In addition, it is found that the relative deviations gradually decrease as the supply voltages rise. After the supply voltages are cut off, different clamping forces drop at different rates, but finally the residual clamping forces keep constant and are almost equal, regardless of different initial voltages. Nevertheless, the decaying time of the clamping force for Coulomb type is much longer than that for J–R type. During the decline of the curves, the calculated residual forces are less than the measured ones at the same moment. It is noted that the prediction precisions of both steady-state clamping force and residual clamping force for J–R type are usually lower than those for Coulomb type. Furthermore, the sources of error are discussed and the reasons or mechanisms of the above phenomena are explained. In summary, the comparisons show that the calculations agree with the measurements within an acceptable error range. It is therefore concluded that the proposed theoretical model is feasible and effective for simulating the characteristics of the residual clamping force for both types of electrostatic chucks. Also, further research for this subject is necessary.

Acknowledgement

The authors would like to thank Mr Yin Zhong of Tsinghua University for his valuable assistance in preliminary experimental plan.

Declaration of Conflicting Interests

The author(s) declared no potential conflicts of interest with respect to the research, authorship, and/or publication of this article.

Funding

The author(s) disclosed receipt of the following financial support for the research, authorship, and/or publication of this article: This work was supported by No.02 National Science and Technology Major Project of China (2011ZX02403-004).

ORCID iD

Kesheng Wang http://orcid.org/0000-0002-1724-2626

References

1. Wright DR, Chen L, Federlin P, et al. Manufacturing issues of electrostatic chucks. *J Vacuum Sci Technol B* 1995; 13: 1910–1916.
2. Wright DR, Hartman DC, Sridharan UC, et al. Low temperature etch chuck: Modeling and experimental results of heat transfer and wafer temperature. *J Vacuum Sci Technol A* 1992; 10: 1065–1070.
3. Meyer JA, Kirmse KHR, Jenq JS, et al. Experiments with back side gas cooling using an electrostatic wafer

holder in an electron cyclotron resonance etching tool. *Appl Phys Lett* 1994; 64: 1926–1928.
4. Shan H, Pu BY, Gao H, et al. Process kit and wafer temperature effects on dielectric etch rate and uniformity of electrostatic chuck. *J Vacuum Sci Technol B* 1996; 14: 521–526.
5. Kalkowski G, Peschel T, Hassall G, et al. Investigations into an electrostatic chuck design for 450 mm Si wafer. In: *Proceedings of SPIE 8324, metrology, inspection, and process control for microlithography XXVI*, San Jose, USA, 12 February 2012, paper no. 83242Z, pp.1–9. Bellingham: SPIE.
6. Hartsough LD. Electrostatic wafer holding. *Solid State Technol* 1993; 36: 87–90.
7. Field J. Electrostatic wafer clamping for next-generation manufacturing. *Solid State Technol* 1994; 37: 91–93.
8. Daviet JF, Peccoud L and Mondon F. Electrostatic clamping applied to semiconductor plasma processing I. Theoretical modeling. *J Electrochem Soc* 1993; 140: 3245–3256.
9. Johnsen A and Rahbek K. A physical phenomenon and its applications to telegraphy, telephony, etc. *J Instn Electr Engrs* 1923; 61: 713–725.
10. Balakrishnan C. Johnsen-Rahbek effect with an electronic semi-conductor. *Brit J Appl Phys* 1950; 1: 211–213.
11. Watanabe T, Kitabayashi T and Nakayama C. Electrostatic force and absorption current of alumina electrostatic chuck. *Japanese J Appl Phys* 1992; 31: 2145–2150.
12. Watanabe T, Kitabayashi T and Nakayama C. Relationship between electrical resistivity and electrostatic force of alumina electrostatic chuck. *Japanese J Appl Phys* 1993; 32: 864–871.
13. Li CH, Chiu YF, Yu YH, et al. Simulation studies on bipolar electrostatic chucks. In: *2015 10th international microsystems, packaging, assembly and circuits technology conference*, Taipei, Taiwan, 21–23 October 2015, paper no. CFP1559B, pp.382–385. New York: IEEE.
14. Shim G II and Sugai H. Temporal analysis of electrostatic chuck characteristics in inductively coupled plasma. *Plasma Fusion Res* 2008; 3: 028.
15. Qin S and McTeer A. Wafer dependence of Johnsen–Rahbek type electrostatic chuck for semiconductor processes. *J Appl Phys* 2007; 102: 064901.
16. Yatsuzuka K, Hatakeyama F, Asano K, et al. Fundamental characteristics of electrostatic wafer chuck with insulating sealant. *IEEE Trans Ind Appl* 2000; 36: 510–516.
17. Yatsuzuka K, Toukairin J, Asano K, et al. Electrostatic chuck with a thin ceramic insulation layer for wafer holding. In: *2001 IEEE industry applications conference. Thirty-sixth IAS annual meeting*, Chicago, USA, 30 September to 4 October 2001, paper no. 7081566, pp.399–403. New York: IEEE.
18. Asano K, Hatakeyama F and Yatsuzuka K. Fundamental study of an electrostatic chuck for silicon wafer handling. *IEEE Trans Ind Appl* 2002; 38: 840–845.
19. Kanno S and Usui T. Generation mechanism of residual clamping force in a bipolar electrostatic chuck. *J Vacuum Sci Technol B* 2003; 21: 2371–2377.
20. Kanno S, Kato K, Yoshioka K, et al. Prediction of clamping pressure in a Johnsen-Rahbek-type electrostatic chuck based on circuit simulation. *J Vacuum Sci Technol B* 2006; 24: 216–223.
21. Shim G II and Sugai H. Dechuck operation of Coulomb type and Johnsen-Rahbek type of electrostatic chuck used in plasma processing. *Plasma Fusion Res* 2008; 3: 051.
22. Lee CY, Lai CS, Yang CM, et al. Residual clamping force and dynamic random access memory data retention improved by gate tungsten etch dechucking condition in a bipolar electrostatic chuck. *Japanese J Appl Phys* 2012; 51: 086502.
23. Sun YC, Cheng J, Lu YJ, et al. Design space of electrostatic chuck in etching chamber. *J Semicond* 2015; 36: 084004.
24. Holm R. *Electric contacts theory and application*. Berlin/Heidelberg/New York: Springer, 1967.
25. Nakasuji M and Shimizu H. Low voltage and high speed operating electrostatic wafer chuck. *J Vacuum Sci Technol A* 1992; 10: 3573–3578.
26. Wang KS, Cheng J, Zhong Y, et al. A novel measuring method of clamping force for electrostatic chuck in semiconductor devices. *J Semicond* 2016; 37: 044012.
27. Stuckes AD. Some theoretical and practical considerations of the Johnsen-Rahbek effect. *Proc Instn Electr Engrs Part B* 1956; 103: 125–131.
28. Atkinson R. A simple theory of the Johnsen-Rahbek effect. *J Phys D: Appl Phys* 1969; 2: 325–332.